

A New Measure of Coarseness for Solutions to Cahn–Hilliard Equations

Peter Howard [†] Adam Larios [‡] Quyuan Lin [§]

January 22, 2026

Abstract

We introduce a new measure of coarseness for characterizing phase separation processes such as those described by Cahn–Hilliard equations. An advantage of our measure is that it remains consistent throughout the evolution, including for solutions with no periodic structure. We use our measure to compare two previous models of coarsening dynamics with numerically generated dynamics, providing the first direct check that we are aware of for the efficacy of these methods.

Keywords: Cahn–Hilliard equation, coarsening dynamics, phase separation, spinodal decomposition.

1 Introduction

For processes of phase separation such as those modeled by Cahn–Hilliard equations, solutions are typically viewed as evolving from less coarse states (e.g., from nearly homogeneous mixtures) to more coarse states (e.g., to fully separated mixtures). The rates at which such processes evolve are of critical importance both for understanding the nature of the processes and for applications, and in order to study these rates it is necessary to have a consistent and effective measure of coarseness that can be employed throughout the phase separation process. Perhaps the earliest such measure was introduced by J. S. Langer in [17]. Noting that late-stage solutions to 1D Cahn–Hilliard equations are nearly periodic, Langer

^{*}MSC 2020: 35Q35, 76T99, 76D05, 35Q30

[†]Corresponding author; Department of Mathematics, Texas A&M University, College Station, TX 77843, USA, phoward@tamu.edu

[‡]Department of Mathematics, University of Nebraska–Lincoln, Lincoln, NE 68588-0130, USA, alarios@unl.edu

[§]School of Mathematical and Statistical Sciences, Clemson University, Clemson, SC 29634, USA, quyuanyl@clemson.edu

suggested using the approximate period, appropriately defined, as a measure of coarseness. Moreover, by combining this measure of coarseness with an approach to evolution based on perturbations instigated by thermal fluctuation in the materials under consideration, Langer was able to arrive at an elegant analytical formula for the time evolution of coarseness in solutions to Cahn–Hilliard equations.

Motivated by Langer’s work, the first author of the current study has introduced an alternative analytical approach to coarsening dynamics based on the spectrum associated with certain unstable periodic stationary solutions to Cahn–Hilliard equations [15]. By utilizing exact periodic solutions rather than asymptotically approximate periodic solutions, this latter approach extends Langer’s method to earlier stages of the coarsening process, providing additional information about the transition from mid-stage dynamics to late-stage dynamics. Nonetheless, there remains a critical period of minimal coarseness during which neither method reasonably applies. Indeed, since both methods rely on periodicity of some form in order for the measure of coarseness to be defined, it is reasonable to assert that neither method provides meaningful values during the period of minimal coarseness.

An alternative measure of coarseness was introduced by Kohn and Otto in [16] in the multidimensional case (Definition 1 from p. 383 of [16]). Translated to the current one-dimensional setting, this measure can be expressed as follows.

Definition 1.1. *For any function $\phi(x)$ periodic on $[-L, +L]$ with mean value 0, the Kohn–Otto length is defined to be*

$$\ell_{KO} := \sup \left\{ \frac{1}{2L} \int_{-L}^{+L} \phi(x) \zeta(x) dx : \zeta \in C^1([-L, +L]) \text{ periodic with } \sup_{x \in [-L, +L]} |\zeta'(x)| \leq 1 \right\}.$$

The clear advantage of the Kohn–Otto length over Langer’s measure is that it readily generalizes to the multidimensional setting. Nonetheless, it retains dependence on periodicity, and so is not suitable for effectively capturing early-stage dynamics.

The primary goal of the current analysis is to introduce a new measure of coarseness in the 1D setting that agrees closely with Langer’s when solutions are nearly periodic, but can be naturally extended throughout the entirety of the coarsening process. This new measure allows us to compare the analytic methods of [17] and [15] with computational results, and better gauge the regions of efficacy for these methods. More generally, our measure of coarseness opens the door for robust studies of coarsening rates not only for Cahn–Hilliard equations, but for systems as well, such as Cahn–Hilliard–Navier–Stokes couplings—an avenue the authors will explore in a subsequent study.

The remainder of the paper is organized as follows. In Section 2, we collect observations about Cahn–Hilliard equations that will be important to our later study, and in Section 3 we use the observations to introduce our measure of coarseness. In Section 4, we review and compare the coarsening rates computed in [17] and [15], and in Section 5 we use our new measure of coarseness to make comparisons with numerically generated rates. In this way, we are able to determine the timescales on which the analytic approaches are most

effectively. We conclude with a discussion of future work, and relegate two technical proofs to a short appendix.

2 Cahn–Hilliard Equations

In this section, we set the stage for our analysis by reviewing some key properties of Cahn–Hilliard equations,

$$\phi_t = \left(M(\phi)(-\kappa\phi_{xx} + F'(\phi))_x \right)_x, \quad (2.1)$$

where $\kappa > 0$ and for this discussion we will make the following assumptions on M and F .

(A) $M \in C^2(\mathbb{R})$, and there exists a constant $m_0 > 0$ so that with $M(\phi) \geq m_0$ for all $\phi \in \mathbb{R}$ (i.e., non-degenerate mobility); $F \in C^4(\mathbb{R})$ has a double-well form: there exist real numbers $\alpha_1 < \alpha_2 < \alpha_3 < \alpha_4 < \alpha_5$ so that F is strictly decreasing on $(-\infty, \alpha_1)$ and (α_3, α_5) and strictly increasing on (α_1, α_3) and $(\alpha_5, +\infty)$, and additionally F is concave up on $(-\infty, \alpha_2) \cup (\alpha_4, +\infty)$ and concave down on (α_2, α_4) .

Remark 2.1. *With its origins in the work of John W. Cahn and John E. Hilliard, especially [2, 3], equation (2.1) is now well established as a foundational model of phase separation dynamics. Although a general review of references on (2.1) is far beyond the scope of this discussion, we mention that our approach and methods are closely related to the work on initiation of phase separation in [11, 12], the analyses of periodic solutions in [14, 15], the analyses of kink and antikink solutions in [1, 4, 13, 20], and the analyses of coarsening rates in [15, 17, 22].*

We observe at the outset that for each F satisfying Assumptions **(A)**, there exists a unique pair of values ϕ_1 and ϕ_2 (the *binodal* values) so that

$$F'(\phi_1) = \frac{F(\phi_2) - F(\phi_1)}{\phi_2 - \phi_1} = F'(\phi_2)$$

and such that the line passing through $(\phi_1, F(\phi_1))$ and $(\phi_2, F(\phi_2))$ lies entirely on or below F . (See Figure 1.) Also, we note that for any linear function $G(\phi) = A\phi + B$ we can replace $F(\phi)$ in (2.1) with $H(\phi) = F(\phi) - G(\phi)$ without changing the equation in any way. If we choose

$$G(\phi) := \frac{F(\phi_2) - F(\phi_1)}{\phi_2 - \phi_1}(\phi - \phi_1) + F(\phi_1),$$

then $H(\phi)$ has local minima at the binodal values, with $H(\phi_1) = H(\phi_2) = 0$, and a local maximum at the unique value ϕ_h for which

$$F'(\phi_h) = \frac{F(\phi_2) - F(\phi_1)}{\phi_2 - \phi_1} \quad \text{and} \quad F''(\phi_h) < 0.$$

Finally, upon replacing ϕ with $\phi + \phi_h$ we can shift H so that the local maximum is located at $\phi_h = 0$. For the remainder of our analysis we will assume that these transformations have been carried out, and we will denote the resulting function F . The standard form that we will use for numerical computations and some specific analytical results is

$$F(\phi) = \frac{1}{4}\alpha\phi^4 - \frac{1}{2}\beta\phi^2 + \frac{1}{4}\frac{\beta^2}{\alpha} = \frac{\alpha}{4} \left(\phi^2 - \frac{\beta}{\alpha} \right)^2, \quad (2.2)$$

which clearly satisfies our general assumptions for all $\alpha, \beta > 0$.

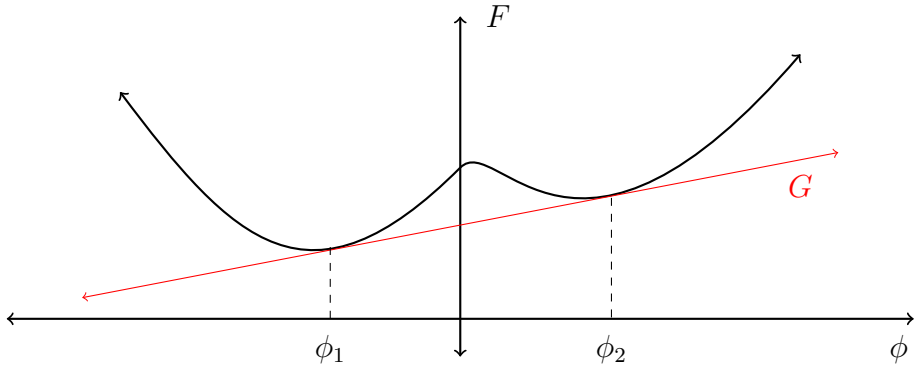


Figure 1: The bulk free energy F along with its supporting line.

Remark 2.2. For convenient reference, we summarize the properties that F will have after the transformations described above: $F \in C^4(\mathbb{R})$, and there exist values $\phi_1 < \phi_3 < 0 < \phi_4 < \phi_2$ so that F is strictly decreasing on $(-\infty, \phi_1)$ and $(0, \phi_2)$ and strictly increasing on $(\phi_1, 0)$ and $(\phi_2, +\infty)$; F is convex on $(-\infty, \phi_3)$ and $(\phi_4, +\infty)$, and concave on (ϕ_3, ϕ_4) ; F has local minima at ϕ_1 and ϕ_2 with $F(\phi_1) = F(\phi_2) = 0$, and F has a local maximum at $\phi = 0$.

2.1 The Cahn–Hilliard energy

Equations of form (2.1) are based on the energy functional

$$E(\phi) := \int_{-L}^{+L} F(\phi) + \frac{\kappa}{2} \phi_x^2 dx, \quad (2.3)$$

introduced for this context in [3] (see also [8, 16]). In particular, (2.1) can be expressed as a conservation law,

$$\phi_t + J_x = 0,$$

with flux

$$J = -M(\phi) \partial_x \frac{\delta E}{\delta \phi},$$

where $\frac{\delta E}{\delta \phi}$ denotes the usual variational gradient, and we have restricted the expressions from [3] to one space dimension. A straightforward calculation shows that if ϕ evolves according to (2.1) then the energy $E(\phi)$ will generally dissipate as it approaches a global minimum value, corresponding with a stationary solution of (2.1). One important aspect of such solutions is the rate at which they coarsen from an initial near-homogeneous configuration to a distinctive non-homogeneous configuration corresponding with an asymptotic limit. In principle, we would like to gauge such coarsening by evolving some designated length scale $\ell(t)$, but in practice it is problematic to consistently assign such a scale to an arbitrary solution $\phi(x, t)$ of (2.1). Instead, it is often more convenient to gauge coarsening by evolution of the energy (2.3), and one goal of the current analysis is to relate the evolution of $E(\phi(\cdot, t))$ to the evolution of a length scale $\ell(t)$ in a consistent manner.

2.2 Periodic solutions of Cahn–Hilliard equations

For many phase separation processes, including the well-studied process of spinodal decomposition, we expect $\phi(x, 0) = \phi_0(x)$ to be a small random perturbation of a homogeneous state $\phi_h = \text{constant}$. We can understand the initiation of phase separation by linearizing (2.1) about this state ($\phi = \phi_h + v$) to obtain the linear perturbation equation

$$v_t = -M(\phi_h)\kappa v_{xxxx} + M(\phi_h)F''(\phi_h)v_{xx}.$$

If we look for solutions of the form $v(x, t) = e^{\lambda t + i\xi x}$ we obtain the dispersion relation

$$\lambda(\xi) = -\kappa M(\phi_h)\xi^4 - M(\phi_h)F''(\phi_h)\xi^2,$$

with leading eigenvalue

$$\lambda_s = \frac{M(\phi_h)F''(\phi_h)^2}{4\kappa} > 0; \quad \text{at} \quad \xi_s = \sqrt{-\frac{F''(\phi_h)}{2\kappa}},$$

and associated period

$$p_s = 2\pi \sqrt{\frac{2\kappa}{-F''(\phi_h)}}, \quad (2.4)$$

where we emphasize that under our assumptions on F , $F''(\phi_h) < 0$. Accordingly, we expect solutions of (2.1), initialized by small random perturbations of ϕ_h , to rapidly evolve toward a periodic solution with period p_s . Indeed, for the case of (2.1) posed on a bounded domain in \mathbb{R} , this expectation has been rigorously verified by Grant [11, 12]. It is natural to view these initial dynamics as culminating once solutions are nearly periodic with period p_s , and we refer to the dynamics up to this time as the *spinodal phase* of the process. Correspondingly, we refer to p_s as the *spinodal period*.

At the end of the spinodal phase, solutions will generally be near a stationary periodic solution with period p_s , and in order to understand the next phase of the dynamics, we

consider the behavior of solutions initialized as perturbations of stationary periodic solutions. As a starting point for this, we have from [14, 15] that there exists a continuum of such periodic solutions $\bar{\phi}(x)$ to (2.1) in the following sense: if ϕ_1 and ϕ_2 denote the binodal values and ϕ_{\min} and ϕ_{\max} are any values so that $\phi_1 < \phi_{\min} < \phi_{\max} < \phi_2$ with additionally

$$F'(\phi_{\min}) > \frac{F(\phi_{\max}) - F(\phi_{\min})}{\phi_{\max} - \phi_{\min}} > F'(\phi_{\max}),$$

then there exists a periodic solution to (2.1) with minimum value ϕ_{\min} and maximum value ϕ_{\max} (see Theorem 1.5 in [14]). Moreover (again from Theorem 1.5 in [14]), we have that if F is as described in Remark 2.2, and if additionally F is an even function (such as (2.2)), then for every amplitude $a \in (0, \phi_2)$ there exists precisely one (up to translation) periodic stationary solution with amplitude a . More precisely, this solution, denoted here $\bar{\phi}(x; a)$, satisfies the relation

$$-\kappa \bar{\phi}_{xx} + F'(\bar{\phi}) = 0 \implies (\bar{\phi}_x)^2 = \frac{2}{\kappa}(F(\bar{\phi}) - F(a)).$$

If we select the shift so that $\bar{\phi}(0; a) = 0$, we find the integral relation

$$\int_0^{\bar{\phi}(x; a)} \frac{dy}{\sqrt{\frac{2}{\kappa}(F(y) - F(a))}} = x, \quad (2.5)$$

from which we see immediately (by symmetry) that $\bar{\phi}(x; a)$ has period

$$p(a) = 4 \int_0^a \frac{dy}{\sqrt{\frac{2}{\kappa}(F(y) - F(a))}}. \quad (2.6)$$

Returning briefly to the initiation of dynamics, we can use (2.6) to compute the minimum possible period, obtained as the limit of $p(a)$ as a tends to 0. For this calculation, we need only observe that for a small and $y \in (0, a)$, we can Taylor expand $F(a)$ about y , and subsequently Taylor expand $F'(y)$ and $F''(y)$ about 0 (and note that $F'(0) = 0$) to write

$$F(y) - F(a) = \frac{1}{2} F''(0)(y^2 - a^2) \left(1 + \mathbf{O}(a)\right).$$

We then have

$$p(a) = 4 \sqrt{\frac{\kappa}{-F''(0)}} \int_0^a \frac{1}{\sqrt{a^2 - y^2}} \left(1 + \mathbf{O}(a)\right) dy = 2\pi \sqrt{\frac{\kappa}{-F''(0)}} + \mathbf{O}(a).$$

We see that the minimum period is

$$p_{\min} := \lim_{a \rightarrow 0^+} p(a) = 2\pi \sqrt{\frac{\kappa}{-F''(0)}}. \quad (2.7)$$

In the following proposition, we observe that the period $p(a)$ increases as the amplitude a increases. In [15], this result is stated without proof as equation (1.11), and although the short proof is straightforward (as asserted in [15]), we have elected to include it in an appendix for completeness. (See Appendix A.)

Proposition 2.3. *Assume F is as described in Remark 2.2, and also that F is an even function. Then for all $a \in (0, \phi_2)$ the period $p(a)$ specified in (2.6) satisfies*

$$p'(a) = \frac{2\sqrt{2\kappa}}{\sqrt{F(0) - F(a)}} - \sqrt{2\kappa} \int_0^a \frac{F'(y) - F'(a)}{(F(y) - F(a))^{3/2}} dy.$$

In addition, if $F'''(\phi) > 0$ for all $\phi \in (0, \phi_2)$ then $p'(a) > 0$ for all $a \in (0, \phi_2)$.

Since p is monotonically increasing as a function of amplitude, we can uniquely specify the spinodal amplitude a_s so that $p(a_s) = p_s$. Precisely, we obtain the relation

$$\frac{2\pi\sqrt{2\kappa}}{\sqrt{-F''(0)}} = 4\sqrt{\kappa} \int_0^{a_s} \frac{dy}{\sqrt{2(F(y) - F(a_s))}},$$

and since $\sqrt{\kappa}$ can be divided out of both sides, we see that a_s does not depend on κ .

Using (2.5), we can identify the unique (up to shift, selected by $\bar{\phi}(0; a_s) = 0$) periodic solution of (2.1) with amplitude a_s , namely $\bar{\phi}(x; a_s)$, and subsequently we define the spinodal energy E_s as the energy associated with this periodic solution,

$$E_s := E(\bar{\phi}(\cdot; a_s)).$$

For the long-time models discussed below, we will typically think of initiating the dynamics once the energy has reduced to the spinodal value.

Although the energy function $E(\phi(\cdot, t))$ can achieve any value attainable via functions $\phi(x, t)$ in its domain, the dynamics we have in mind involve solutions with energies less than the energy achieved by the homogeneous configuration $\phi_0 \equiv 0$. For a given interval $[-L, +L]$, this is easily computed to be

$$E_{\max} := E(0) = \int_{-L}^{+L} F(0) dx = 2LF(0). \quad (2.8)$$

As time increases, energies will decrease as solutions approach either a kink or anti-kink solution, respectively $K(x)$ or $K(-x)$, where

$$-\kappa K'' + F'(K) = 0, \quad \forall x \in \mathbb{R},$$

with also

$$\lim_{x \rightarrow -\infty} K(x) = \phi_1, \quad \lim_{x \rightarrow +\infty} K(x) = \phi_2.$$

(See [14] for existence of such solutions, and [13] for asymptotic stability; we note that according to convention (see, e.g., [5]), a *kink* solution is monotonically increasing, while an *anti-kink* solution is monotonically decreasing.) These solutions provide us with a lower bound on the energy

$$E_{\min} := \int_{-L}^{+L} F(K(x)) + \frac{\kappa}{2} |K'(x)|^2 dx,$$

which will be computed explicitly in Proposition 2.4 just below.

For specific implementations of our approach, we will use the family of bulk free energy densities specified in (2.2). Many of the preceding relations can be made explicit in this case, and for convenient reference we summarize these in Proposition 2.4 just below. Several of the statements in this proposition are taken or adapted from the references [13, 14, 15], and others are straightforward calculations, so the short proof is relegated to Appendix A.

Proposition 2.4. *For (2.1), let M satisfy the assumptions in (A), and let F be as in (2.2). Then the following hold:*

(i) **Minimum period.** *The minimum period computed in (2.7) is $p_{\min} = 2\pi\sqrt{\kappa/\beta}$, and the associated energy computed in (2.8) is $E_{\max} = L\beta^2/(2\alpha)$.*

(ii) **Spinodal period.** *The spinodal period computed in (2.4) is $p_s = 2\pi\sqrt{2\kappa/\beta}$.*

(iii) **Periodic solutions.** *For each $a \in (0, \sqrt{\beta/\alpha})$, the periodic solution $\bar{\phi}(x; a)$ specified in (2.5) can be expressed as a Jacobi elliptic function*

$$\bar{\phi}(x; a) = a \operatorname{sn} \left(\sqrt{\frac{-2(F(a) - F(0))}{\kappa}} \frac{x}{a}, k \right), \quad (2.9)$$

where

$$k = \sqrt{-\frac{\alpha a^4}{4(F(a) - F(0))}}. \quad (2.10)$$

(iv) **Kink solutions and the minimum energy.** *The binodal values for F are $\pm\sqrt{\beta/\alpha}$, and there exists a unique (up to translation) kink solution of (2.1),*

$$K(x) = \sqrt{\frac{\beta}{\alpha}} \tanh \left(\sqrt{\frac{\beta}{2\kappa}} x \right). \quad (2.11)$$

The energy associated with this kink solution on $[-L, +L]$ is

$$E_{\min} := E(K(x)) = \int_{-L}^{+L} F(K(x)) + \frac{\kappa}{2} K'(x)^2 dx = \sqrt{2\kappa\alpha} K(L) \left(\frac{\beta}{\alpha} - \frac{K(L)^2}{3} \right), \quad (2.12)$$

and it follows that

$$E_{\min}^{\infty} := \lim_{L \rightarrow \infty} E_{\min} = \frac{2\beta^2}{3\alpha} \sqrt{\frac{2\kappa}{\beta}}.$$

Remark 2.5. For the periodic solution (2.9), $\text{sn}(y; k)$ denotes the Jacobi elliptic function, defined so that

$$\text{sn}(y; k) = \sin \theta; \quad \text{where} \quad y = \int_0^\theta \frac{d\zeta}{\sqrt{1 - k^2 \sin^2 \zeta}}.$$

For implementations, we evaluate $\text{sn}(y; k)$ with the MATLAB function `ellipj.m`. The period in this case is

$$p(a) = \frac{4a\sqrt{\kappa}}{\sqrt{-2(F(a) - F(0))}} \mathcal{K}(k),$$

where \mathcal{K} denotes the complete elliptic integral

$$\mathcal{K}(k) = \int_0^1 \frac{ds}{\sqrt{(1 - s^2)(1 - k^2 s^2)}}.$$

For implementations, we evaluate $\mathcal{K}(k)$ with the MATLAB function `ellipke.m`.

Remark 2.6. We observe for consistency that the expression in (iii) for $\bar{\phi}(x; a)$, $a \in (0, \sqrt{\frac{\beta}{\alpha}})$, matches the results when $a \rightarrow 0$ and $a \rightarrow \sqrt{\frac{\beta}{\alpha}}$. To see this, we first take $a \rightarrow 0$ and observe that

$$\lim_{a \rightarrow 0} \sqrt{\frac{-2(F(a) - F(0))}{a^2 \kappa}} x = \sqrt{\frac{\beta}{\kappa}} x \quad \text{and} \quad \lim_{a \rightarrow 0} k = \lim_{a \rightarrow 0} \sqrt{\frac{-\alpha a^4}{4(F(a) - F(0))}} = 0.$$

As $\text{sn}(u; 0) = \sin u$, one can conclude that

$$\lim_{a \rightarrow 0} \bar{\phi}(x; a) = \lim_{a \rightarrow 0} a \sin\left(\sqrt{\frac{\beta}{\kappa}} x\right) = 0.$$

Next, taking $a \rightarrow \sqrt{\frac{\beta}{\alpha}}$ we find that

$$\lim_{a \rightarrow \sqrt{\frac{\beta}{\alpha}}} \sqrt{\frac{-2(F(a) - F(0))}{a^2 \kappa}} x = \sqrt{\frac{\beta}{2\kappa}} x \quad \text{and} \quad \lim_{a \rightarrow \sqrt{\frac{\beta}{\alpha}}} k = \lim_{a \rightarrow \sqrt{\frac{\beta}{\alpha}}} \sqrt{\frac{-\alpha a^4}{4(F(a) - F(0))}} = 1.$$

As $\text{sn}(u; 1) = \tanh u$, we obtain

$$\lim_{a \rightarrow \sqrt{\frac{\beta}{\alpha}}} \bar{\phi}(x; a) = \sqrt{\frac{\beta}{\alpha}} \text{sn}\left(\sqrt{\frac{\beta}{2\kappa}} x, 1\right) = \sqrt{\frac{\beta}{\alpha}} \tanh\left(\sqrt{\frac{\beta}{2\kappa}} x\right) = K(x).$$

which gives the kink solution.

As a working example for quantitative analysis, we will take $M(\phi) \equiv 1$ and use F as in (2.2) with $\alpha = \beta = 1$, leaving only κ to vary. The choice of constant mobility is made because qualitative dynamics do not vary much as long as the mobility is non-degenerate. As a baseline case, we will take $\kappa = 0.001$. Using these values, periodic solutions with three different periods are depicted in Figure 2.

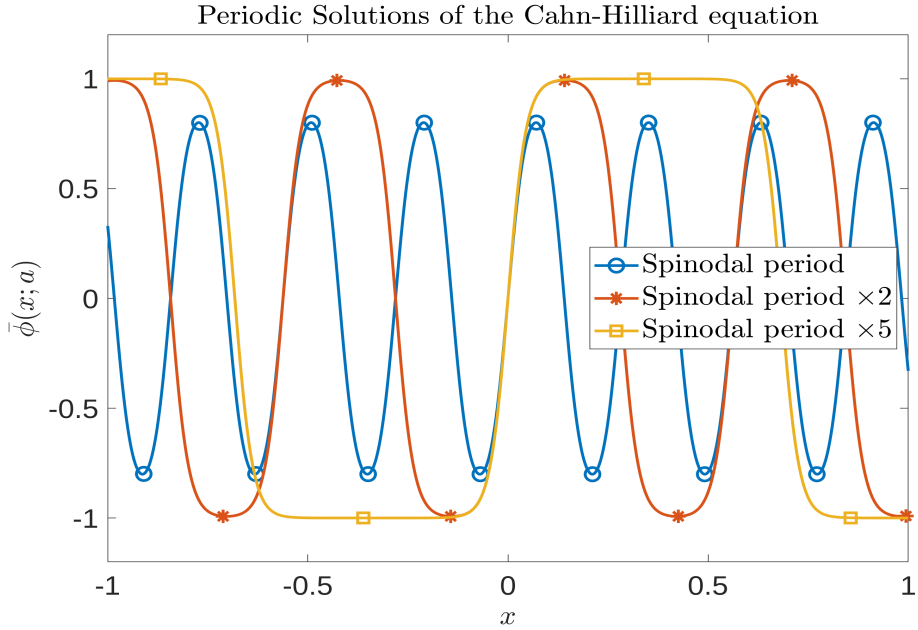


Figure 2: Periodic solutions for the Cahn–Hilliard equation. Note that the domain $[-1, 1]$ is depicted for visual clarity, but by Proposition 2.4 (ii, the periods p_s are approximately 0.2810, 0.5620, and 1.4050.

3 A New Measure of Coarseness

We return now to our goal set out previously of relating each energy $e \in (E_{\min}, E_{\max})$ with an associated length scale ℓ . Since solutions to (2.1) tend to be near periodic solutions during a substantial portion of the evolution, our strategy will be to identify with a given energy e the period p for which

$$E(\bar{\phi}(\cdot; a(p))) = e.$$

One caveat for this approach is that the function

$$\mathcal{E}(p) := E(\bar{\phi}(\cdot; a(p))) = \int_{-L}^{+L} F(\bar{\phi}(x; a(p))) + \frac{\kappa}{2} \bar{\phi}_x(x; a(p))^2 dx \quad (3.1)$$

is not invertible, a point we clarify in the next proposition.

Proposition 3.1. *For (2.1), let M satisfy the assumptions in (A), and let F be as in (2.2). Then the function $\mathcal{E}(p)$ defined in (3.1) is not invertible on $[p_{\min}, \infty)$.*

Proof. First, since the period p depends monotonically on the amplitude a , we can work with the map

$$E(a) := E(\bar{\phi}(\cdot; a)) = \int_{-L}^{+L} F(\bar{\phi}(x; a)) + \frac{\kappa}{2} \bar{\phi}_x(x; a)^2 dx.$$

We will prove the proposition by showing that $\mathbb{E}'(a)$ does not have a fixed sign. Upon differentiating \mathbb{E} in a , we obtain

$$\begin{aligned} \frac{d\mathbb{E}}{da}(a) &= \int_{-L}^{+L} F'(\bar{\phi}(x; a))\bar{\phi}_a(x; a) + \kappa\bar{\phi}_x(x; a)\bar{\phi}_{xa}(x; a)dx \\ &\stackrel{\text{parts}}{=} \int_{-L}^{+L} F'(\bar{\phi}(x; a))\bar{\phi}_a(x; a) - \kappa\bar{\phi}_{xx}(x; a)\bar{\phi}_a(x; a)dx \\ &\quad + \kappa\bar{\phi}_x(L; a)\bar{\phi}_a(L; a) - \kappa\bar{\phi}_x(-L; a)\bar{\phi}_a(-L; a) \\ &= \kappa\bar{\phi}_x(L; a)\bar{\phi}_a(L; a) - \kappa\bar{\phi}_x(-L; a)\bar{\phi}_a(-L; a), \end{aligned} \quad (3.2)$$

where the final equality follows because $-\kappa\bar{\phi}_{xx}(x; a) + F'(\bar{\phi}(x; a)) = 0$ for a periodic wave $\bar{\phi}(x; a)$.

In order to understand the derivative $\bar{\phi}_a(x; a)$, we recall the explicit form for $\bar{\phi}(x; a)$,

$$\bar{\phi}(x; a) = a \operatorname{sn}(h(a)x; k), \quad h(a) = \frac{1}{a} \sqrt{\frac{-2(F(a) - F(0))}{\kappa}}. \quad (3.3)$$

With F as specified in (2.2), we find that

$$F(a) - F(0) = a^2 \left(\frac{\alpha}{4} a^2 - \frac{\beta}{2} \right),$$

so

$$h(a) = \sqrt{\frac{\alpha}{2\kappa}} \sqrt{\frac{2\beta}{\alpha} - a^2}, \quad h'(a) = -\frac{\sqrt{\frac{\alpha}{2\kappa}} a}{\sqrt{\frac{2\beta}{\alpha} - a^2}}.$$

Now,

$$\bar{\phi}_a(x; a) = \operatorname{sn}(h(a)x; k) + a \operatorname{sn}'(h(a)x; k)h'(a)x,$$

and likewise

$$\bar{\phi}_x(x; a) = a \operatorname{sn}'(h(a)x; k)h(a),$$

from which we can write

$$\bar{\phi}_a(x; a) = \frac{1}{a} \bar{\phi}(x; a) + \frac{h'(a)x}{h(a)} \bar{\phi}_x(x; a) = \frac{1}{a} \bar{\phi}(x; a) - \frac{ax}{\frac{2\beta}{\alpha} - a^2} \bar{\phi}_x(x; a).$$

From these considerations, we see that

$$\bar{\phi}_x(x; a)\bar{\phi}_a(x; a) = \frac{1}{a} \bar{\phi}(x; a)\bar{\phi}_x(x; a) - \frac{ax}{\frac{2\beta}{\alpha} - a^2} \bar{\phi}_x(x; a)^2.$$

Since $\bar{\phi}(x; a)$ is an odd function (because $\operatorname{sn}(x; k)$ is odd), we see that the product $\bar{\phi}_x(x; a)\bar{\phi}_a(x; a)$ is an odd function, and from this we can conclude from (3.2) that

$$\begin{aligned} \frac{d\mathbb{E}}{da}(a) &= 2\kappa\bar{\phi}_x(L; a)\bar{\phi}_a(L; a) = \frac{2\kappa}{a} \bar{\phi}(L; a)\bar{\phi}_x(L; a) - \frac{2\kappa a L}{\frac{2\beta}{\alpha} - a^2} \bar{\phi}_x(L; a)^2 \\ &= \frac{2\kappa}{a} \bar{\phi}_x(L; a) \left(\bar{\phi}(L; a) - \frac{a^2 L}{\frac{2\beta}{\alpha} - a^2} \bar{\phi}_x(L; a) \right). \end{aligned} \quad (3.4)$$

Recalling that our goal is to understand the sign of $\mathbb{E}'(a)$, as a varies, we begin by considering a configuration in which $\bar{\phi}(L; a) = 0$. In this case,

$$\begin{aligned}\frac{d\mathbb{E}}{da}(a) &= -\frac{2\kappa a L}{\frac{2\beta}{\alpha} - a^2} \bar{\phi}_x(L; a)^2 = -\frac{2\kappa a L}{\frac{2\beta}{\alpha} - a^2} \frac{2}{\kappa} (F(0) - F(a)) \\ &= -\frac{4a L}{\frac{2\beta}{\alpha} - a^2} \frac{\alpha a^2}{4} \left(\frac{2\beta}{\alpha} - a^2 \right) = -a^3 \alpha L < 0.\end{aligned}$$

With this configuration, we have either $\bar{\phi}_x(L; a) < 0$ or $\bar{\phi}_x(L; a) > 0$, and for specificity we will focus on the former case. If we now think about increasing a a small amount, we know from the monotonic dependence of p on a that the period p will increase a small amount and we will have $\bar{\phi}(L; a) > 0$. As the amplitude a continues to increase the value of $\bar{\phi}(L; a)$ will increase, and correspondingly the value of $|\bar{\phi}_x(L; a)|$ will decrease. Nonetheless, for $\bar{\phi}_x(L; a) < 0$ and $\bar{\phi}(L; a) > 0$ we will continue to have $\mathbb{E}'(a) < 0$ until $\bar{\phi}(L; a)$ achieves its maximum value $\bar{\phi}(L; a) = a$, at which point $\mathbb{E}'(a) = 0$ (because $\bar{\phi}_x(L; a) = 0$). As a increases further, we will have $\bar{\phi}_x(L; a) > 0$, with $|\bar{\phi}_x(L; a)|$ sufficiently small so that

$$\bar{\phi}(L; a) - \frac{a^2 L}{\frac{2\beta}{\alpha} - a^2} \bar{\phi}_x(L; a) > 0.$$

Since we are now in the setting with $\bar{\phi}_x(L; a) > 0$, we see from (3.4) that we will have $\mathbb{E}'(a) > 0$. In this way, we conclude that $\mathbb{E}(a)$ is not monotonically decreasing as a increases. Due to the monotonic dependence of a on p , we can additionally conclude that the energy map $\mathcal{E}(p)$ is not monotonic in p , and so is not invertible for all values of p . \square

According to Proposition 3.1, we cannot invert $\mathcal{E}(p)$, but we will see below that the pseudoinverse of $\mathcal{E}(p)$ nonetheless provides an effective measure of coarsening.

Definition 3.2. *Given a fixed energy $e \in (E_{\min}, E_{\max}]$, we define the associated period p to be the pseudoinverse*

$$p = \inf\{\tilde{p} > 0 : \mathcal{E}(\tilde{p}) \leq e\}. \quad (3.5)$$

To better understand why the pseudoinverse works well in this case, we observe that $\mathcal{E}(p)$ is a mostly decreasing function of p except on some small intervals on which $\mathcal{E}'(p)$ is close to 0 (see, e.g., Figure 4). In Figure 3, we plot $\mathcal{E}(p)$ in the case $\alpha = \beta = 1$, $\kappa = 0.001$, and $L = 1$. We see from this plot that as p increases, sharp gradients with $\mathcal{E}'(p) < 0$ alternate with plateaus where $\mathcal{E}'(p) \cong 0$. The sharp gradients occur near values of p for which $\bar{\phi}(L; a(p)) = 0$, as in the proof of Proposition 3.1. Proposition 3.3 addresses the nature of the plateaus.

Proposition 3.3. *For (2.1), let M satisfy the assumptions in (A), and let F be as in (2.2). Then for any $p > p_{\min}$ for which $\mathcal{E}'(p) > 0$, we have the inequality*

$$\mathcal{E}'(p) \leq \frac{a^3 \sqrt{\alpha \kappa} (1 + \delta)^{3/2} \delta^3 (\delta - 1)}{2L},$$

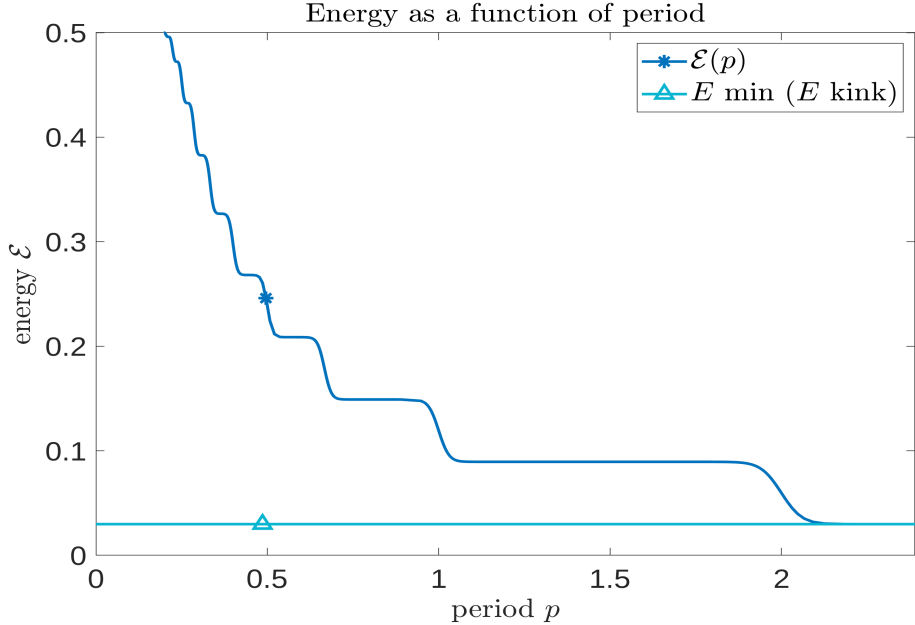


Figure 3: Plot of $\mathcal{E}(p)$, computed with $\alpha = \beta = 1$, $\kappa = 0.001$, and $L = 1$.

where $\delta = \sqrt{2\beta/(\alpha a^2) - 1}$ and a is the unique amplitude corresponding with p .

Proof. Recalling (3.4) from the proof of Proposition 3.1, we see that if $\bar{\phi}_x(L; a) > 0$ then we can only have $\mathbb{E}'(a) > 0$ if

$$\frac{a^2 L}{\frac{2\beta}{\alpha} - a^2} \bar{\phi}_x(L; a) < \bar{\phi}(L; a),$$

so that

$$\bar{\phi}_x(L; a) \leq \frac{\frac{2\beta}{\alpha} - a^2}{a^2 L} \bar{\phi}(L; a).$$

If we substitute this inequality into (3.4), we see that

$$\frac{d\mathbb{E}}{da}(a) \leq \frac{2\kappa}{a} \bar{\phi}_x(L; a) \bar{\phi}(L; a) < \frac{2\kappa}{a} \frac{\frac{2\beta}{\alpha} - a^2}{a^2 L} \bar{\phi}(L; a)^2 \leq \frac{2\kappa}{a} \frac{\frac{2\beta}{\alpha} - a^2}{L}, \quad (3.6)$$

where in obtaining the final inequality we have observed that $|\bar{\phi}(L; a)| \leq a$.

In order to translate this into information about the size of $\mathcal{E}'(p)$, we observe the relation

$$\mathcal{E}'(p) = \mathbb{E}'(a)/p'(a). \quad (3.7)$$

From the proof of Proposition 2.3 (see Appendix A), we know that

$$p'(a) = 2\sqrt{2\kappa} \int_0^1 \frac{G(az) - G(a)}{(F(az) - F(a))^{3/2}} dz, \quad (3.8)$$

where

$$G(y) = F(y) - \frac{y}{2}F'(y),$$

and moreover noted in the same proof that for all $a \in (0, \sqrt{\beta/\alpha})$ we have $p'(a) > 0$ (under the assumptions of that proposition). For our choice of F (2.2), we have the relations

$$\begin{aligned} F(az) - F(a) &= \frac{\alpha a^4}{4}(1 - z^2)(\delta^2 - z^2), \\ G(az) - G(a) &= \frac{\alpha a^4}{4}(1 - z^2)(1 + z^2), \end{aligned}$$

where for notational brevity we have set

$$\delta^2 := \frac{2\beta}{\alpha a^2} - 1,$$

which is greater than 1 for all $a \in (0, \sqrt{\frac{\beta}{\alpha}})$. Upon substituting these relations into (3.8), we arrive at the relation

$$\begin{aligned} p'(a) &= \frac{4\sqrt{2\kappa}}{a^2\sqrt{\alpha}} \int_0^1 \frac{1+z^2}{(1-z^2)^{1/2}(\delta^2-z^2)^{3/2}} dz \\ &= \frac{4\sqrt{2\kappa}}{a^2\sqrt{\alpha}} \int_0^1 \frac{1+z^2}{[(1-z)(1+z)]^{1/2}[(\delta-z)(\delta+z)]^{3/2}} dz. \end{aligned}$$

We are primarily interested in a lower bound on this quantity,

$$\begin{aligned} p'(a) &\geq \frac{4\sqrt{2\kappa}}{a^2\sqrt{\alpha}} \frac{1}{\sqrt{2}(1+\delta)^{3/2}} \int_0^1 \frac{1}{(1-z)^{1/2}(\delta-z)^{3/2}} dz \\ &\geq \frac{4\sqrt{\kappa}}{a^2\sqrt{\alpha}(1+\delta)^{3/2}} \int_0^1 \frac{1}{(\delta-z)^2} dz, \end{aligned}$$

where the second inequality follows immediately from the observation that $\delta > 1$. Integrating directly, we now arrive at the inequality

$$p'(a) \geq \frac{4\sqrt{\kappa}}{a^2\sqrt{\alpha}(1+\delta)^{3/2}} \left(\frac{1}{\delta(\delta-1)} \right). \quad (3.9)$$

The stated estimate on $\mathcal{E}'(p)$ now follows from (3.7), (3.6), and (3.9).

Finally, we recall that these calculations have been carried out under the assumption $\bar{\phi}_x(L; a) > 0$, and note that the case with $\bar{\phi}_x(L; a) < 0$ is similar. \square

Remark 3.4. *As expected, we see from Proposition 3.3 that as the amplitude a tends toward the maximum amplitude $\sqrt{\beta/\alpha}$, $p'(a)$ tends toward ∞ (since δ tends toward 1). I.e., for*

late-stage coarsening, $\mathcal{E}'(p)$ is much smaller than $\mathbb{E}'(a)$. For intermediate values of a , $p'(a)$ is proportional to $\sqrt{\kappa}$, so that $\mathcal{E}'(p)$ is (also) proportional to $\sqrt{\kappa}$.

Although we are primarily interested in intermediate- to late-stage coarsening, it is perhaps interesting to note the behavior of $\mathcal{E}'(p)$ as a tends toward 0 (so p tends toward p_{\min}). As noted previously, in the event that $\mathbb{E}'(a) > 0$, we have the inequality

$$\mathbb{E}'(a) < \frac{2\kappa}{a} \bar{\phi}_x(L; a) \bar{\phi}(L; a).$$

Recalling (3.3), we see that

$$|\bar{\phi}_x(L; a)| \leq a \sqrt{\frac{\beta}{\kappa}},$$

where we have noted that $|\operatorname{sn}'(x; k)| \leq 1$ for all $x \in \mathbb{R}$ (see, e.g., [19]). In this way, we conclude that

$$\mathbb{E}'(a) \leq 2a\sqrt{\beta\kappa}.$$

We can also obtain an alternative lower bound on $p'(a)$,

$$\begin{aligned} p'(a) &= \frac{4\sqrt{2\kappa}}{a^2\sqrt{\alpha}} \int_0^1 \frac{1+z^2}{(1-z^2)^{1/2}(\delta^2-z^2)^{3/2}} dz \\ &\geq \frac{4\sqrt{2\kappa}}{a^2\delta^3\sqrt{\alpha}} \int_0^1 \frac{1}{\sqrt{1-z^2}} dz = \frac{2\pi\sqrt{2\kappa}}{a^2\delta^3\sqrt{\alpha}}. \end{aligned}$$

Combining these observations, we see that

$$\mathcal{E}'(p) = \mathbb{E}'(a)/p'(a) \leq 2a\sqrt{\beta\kappa} \frac{a^2\delta^3\sqrt{\alpha}}{2\pi\sqrt{2\kappa}} = \frac{\sqrt{\alpha\beta}}{\pi\sqrt{2}} \left(\frac{2\beta}{\alpha} - a^2 \right)^{3/2}.$$

We conclude that $\mathcal{E}'(p)$ is bounded above as p approaches p_{\min} , though no longer proportional to $\sqrt{\kappa}$.

We now precisely specify our measure of coarseness.

Definition 3.5. For any solution $\phi(x, t)$ to (2.1) with energy $E(\phi(\cdot, t)) \in (E_{\min}, E_{\max}]$, we define the coarseness ℓ to be the period p defined in (3.5) with $e = E(\phi(\cdot, t))$.

In specifying this notion of coarseness, our focus has been on identifying a measure that can be used in a consistent way from the onset of spinodal decomposition through the late stages of coarsening. The energy (2.3) is often used in precisely this way, but it has the disadvantage that it does not measure actual coarseness (i.e., a characteristic length describing the state of the alloy) at any time during the dynamics. Our approach on the other hand, has the advantages of energy during early-stage dynamics, and is also a genuine measure of coarseness during the later stages of the dynamics. This allows us to study the rate of coarsening dynamics throughout the phase-separation process, and better

understand changes that occur as the process unfolds. We will work with this measure of coarseness throughout the remainder of the analysis.

As an illustration of the considerations discussed in this section, we consider again the specific case of (2.1) with $\kappa = 0.001$, $M(\phi) \equiv 1$, and F as in (2.2) with $\alpha = 1$ and $\beta = 1$. Referring to Figure 3, we pick the plateau between about 0.29 and 0.32, and in Figure 4 we zoom in on this flat section to see that in fact there is a small interval of periods for which monotonicity is lost.

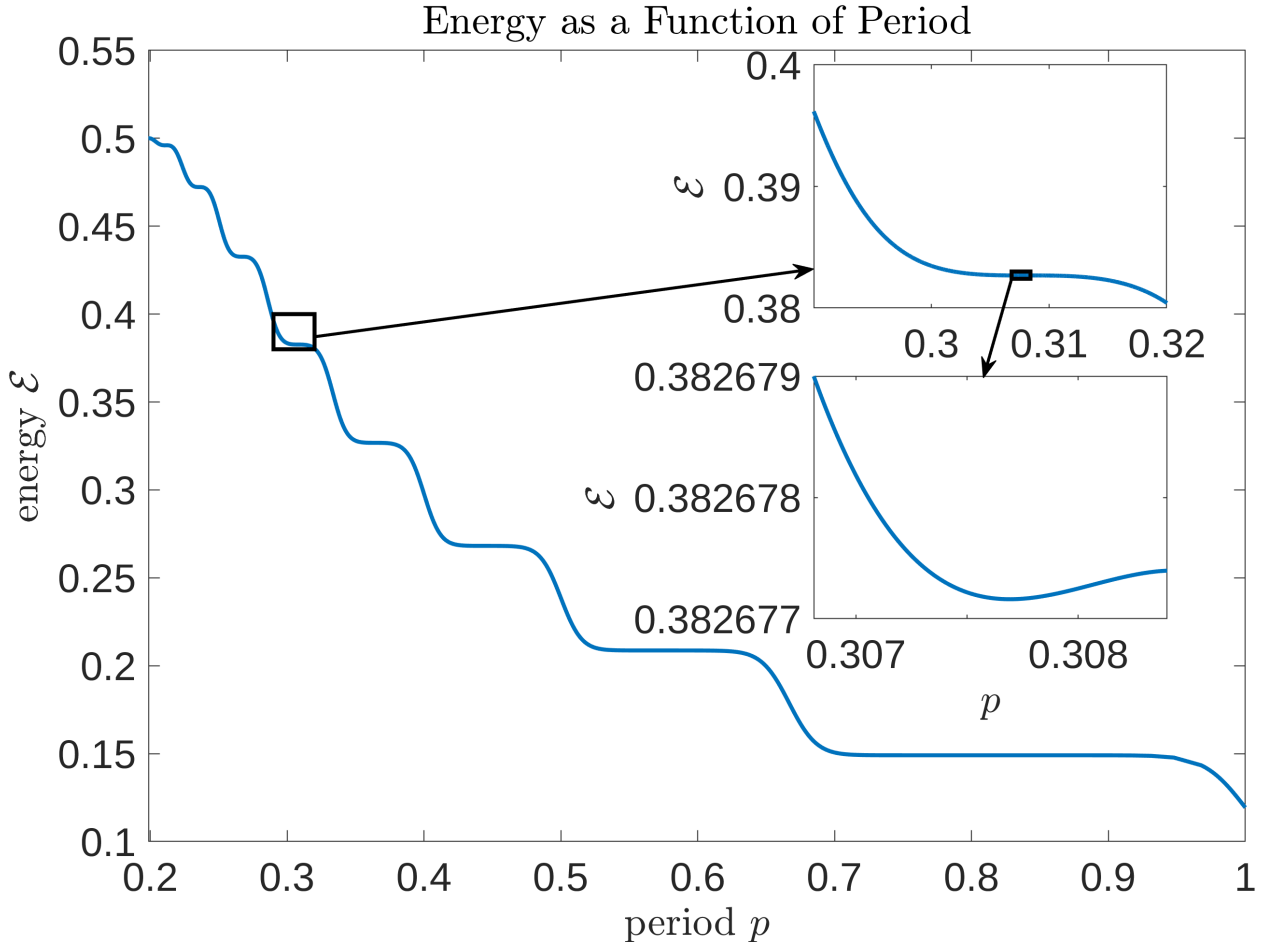


Figure 4: Plot of $\mathcal{E}(p)$, with zoom-ins at $p \in [0.29, 0.32]$ and $p \in [0.3068, 0.3084]$ inset. Computed with $\alpha = \beta = 1$, $\kappa = 0.001$, and $L = 1$. We see that, as discussed in Section 3, $\mathcal{E}(p)$ can briefly lose monotonicity.

We end this section by briefly contrasting our measure of coarseness with the measure introduced by Kohn and Otto in [16], stated above as Definition 1.1. In particular, in the one-dimensional setting, our measure has the following advantages: (1) we can assign a length scale to any function $\phi \in C^1([-L, +L])$ as long as $E(\phi) \in (E_{\min}, E_{\max}]$; (2) since our measure of length is directly linked to solutions of (2.1), it serves as a more precise indicator

of the extent to which the associated solution $\phi(x, t)$ has evolved toward its final asymptotic state; and (3) our measure is more readily computed (by (3.5)).

4 Coarsening Rates Models

In Section 5, we will compare coarsening rates for solutions of (2.1) computed in three different ways: (1) by direct numerical integration of (2.1); (2) by a long-time coarsening model due to Langer [17]; and (3) by a coarsening model due to one of the authors [15]. In preparation for that, we now provide background information on each of these approaches.

Computation. For our direct computations, we will initialize the flow with random perturbations of the homogeneous configuration $\phi_0(x) \equiv 0$. We then solve forward until the energy $E(\phi(x, t))$ reaches the spinodal energy E_s , and it is from this point that we compare energies computed in three different ways.

Langer's relation. In [17], Langer employs a statistical development to capture thermal fluctuations driving phase separation, and arrives at a straightforward equation for the evolution of a coarseness measure ℓ as a function of time. In the current framework, we can interpret equation (6.26) in [17] as an equation for the period p as a function of time,

$$p(t) = p_0 + \sqrt{\frac{2\kappa}{\beta}} \ln \left(1 + \frac{16\beta^2(t - t_0)}{\kappa} e^{-\frac{p_0}{\sqrt{2\kappa/\beta}}} \right). \quad (4.1)$$

Here, we take the period to be p_0 at time t_0 .

Remark 4.1. Equation (6.26) in [17] is

$$\ell(t) = \ell_0 + \frac{\xi}{2} \ln \left(1 + \frac{32t}{\tau_0} e^{-2\ell_0/\xi} \right), \quad (4.2)$$

where $\ell(t) = p(t)/2$ (with $p(t)$ as in the current analysis; see Figure 4 in [17]). In obtaining (4.1), we have chosen Langer's constants Γ , a , d , κ_b , and T so that

$$\frac{\Gamma a^{2+d}}{2\kappa_b T} = 1,$$

in which case equation (3.4) in [17] becomes (in the notation of [17])

$$\bar{\eta}_t = (-\epsilon_0 \xi_0^2 \bar{\eta}_{xx} + F'(\bar{\eta}))_{xx}.$$

In particular, we obtain our equation (2.1) with $M(\phi) \equiv 1$ and $\kappa = \epsilon_0 \xi_0^2$. The combination $\epsilon_0 \xi_0^2$ always appears together in the development of [17], and is replaced below with the constant κ . (Here, we have denoted Boltzmann's constant κ_b to distinguish it from our κ ; Langer denotes it by κ .) In this case, $\tau_0 = 2\kappa/\beta^2$ and $\xi = \sqrt{2\kappa/\beta}$, so that (4.2) becomes

$$\ell(t) = \ell_0 + \sqrt{\frac{\kappa}{2\beta}} \ln \left(1 + \frac{16\beta^2 t}{\kappa} e^{-2\ell_0/\sqrt{2\kappa/\beta}} \right).$$

Our (4.1) is obtained by multiplying this last expression by 2, replacing $2\ell_0$ with p_0 , and allowing the initial time to be $t_0 > 0$. (Langer takes the initial time to be 0 by convention, initiating late-stage dynamics at $t = 0$.)

The approach of [15]. A drawback of Langer's approach in [17] is that approximations are made that require the coarsening process to be at an asymptotically late stage. In particular, Langer approximates late-stage steady-state periodic solutions by piecing together enriched regions with transitions taken from kink and antikink solutions. In [15], this approach is refined by the use of exact periodic solutions $\bar{\phi}(x; a)$ in place of the approximate solutions, with the further advantage that these periodic solutions can serve to approximate the dynamics as early as the spinodal time. Following this replacement of the approximate solutions with exact solutions, the method of [15] follows Langer's approach of linearizing and determining the coarsening rate from the eigenvalues of the resulting eigenvalue problem. Before describing the model obtained in this way, we briefly summarize an efficient method for computing these eigenvalues. First, if (2.1) (with $M \equiv 1$) is linearized about $\bar{\phi}(x; a)$, with $\phi = \bar{\phi} + v$, we obtain the perturbation equation

$$v_t = (-\kappa v_{xx} + F''(\bar{\phi})v)_{xx},$$

and the corresponding eigenvalue problem

$$(-\kappa\psi'' + F''(\bar{\phi})\psi)'' = \lambda\psi. \quad (4.3)$$

As a starting point, we can explicitly compute the right-most eigenvalue for the limiting case with amplitude $a = 0$, corresponding with $\bar{\phi}(x; 0) \equiv 0$. In this case, (4.3) becomes

$$-\kappa\psi''' - \beta\psi'' = \lambda\psi,$$

where we have observed that $F''(0) = -\beta$. Any non-imaginary roots of the characteristic polynomial¹ for this equation correspond to eigenfunctions which are unbounded as $|x| \rightarrow \infty$. Moreover, we rule out repeated-root solutions, since these are necessarily unbounded on \mathbb{R} . Hence, we look for eigenfunctions of the form $\psi(x) = e^{i\xi x}$ for some $\xi \in \mathbb{R}$, which yields

$$-\kappa\xi^4 + \beta\xi^2 = \lambda.$$

We find that the maximum of $\lambda(\xi)$ occurs at $\xi = \pm\sqrt{\beta/(2\kappa)}$, with

$$\lambda_{\max} = \frac{\beta^2}{4\kappa}.$$

For the specific values $\kappa = 0.001$ and $\beta = 1$, this is $\lambda_{\max} = 250$.

¹Note that, even if one looks for eigenfunctions in the space of tempered distributions, after taking the Fourier transform, one finds that the support of $\widehat{\psi}$ is at most four points, corresponding to solutions of the characteristic polynomial. Hence, the only eigenfunctions are given by the characteristic polynomial method.

More generally, in [15] (which adapts the approach of [9, 10] to the current setting), Floquet theory is used to characterize the leading eigenvalue associated with any periodic solution $\bar{\phi}(x; a)$. To understand how this works, we first express the eigenvalue problem (4.3) as a first-order system, setting $y = (y_1, y_2, y_3, y_4)^T$, with $y_j = \psi^{(j)}$, $j = 0, 1, 2, 3$. Then y solves the system

$$y' = \mathbb{A}(x; \lambda)y, \quad \mathbb{A}(x; \lambda) = \begin{pmatrix} 0 & 1 & 0 & 0 \\ 0 & 0 & 1 & 0 \\ 0 & 0 & 0 & 1 \\ (b''(x) - \lambda)/\kappa & 2b'(x)/\kappa & b(x)/\kappa & 0 \end{pmatrix}, \quad (4.4)$$

where $b(x) = F''(\bar{\phi}(x; a))$. We can compute a fundamental matrix for (4.4),

$$\Phi' = \mathbb{A}(x; \lambda)\Phi, \quad \Phi(0; \lambda) = I_4,$$

and the monodromy matrix is defined to be $M(\lambda; p) := \Phi(p; \lambda)$. The Evans function is

$$D(\lambda, \xi) = \det(M(\lambda; p) - e^{i\xi p} I_4),$$

and in this setting λ is an eigenvalue of (4.3) if and only if $D(\lambda, \xi) = 0$ for some $\xi \in \mathbb{R}$. (See [9, 10] for details on the Evans function for periodic solutions generally, and [14, 15] for specialization to the current setting.)

In practice, we can use this to compute leading eigenvalues in the following relatively efficient way. First, we know that for $a = 0$, with corresponding minimum period p_{\min} (from (2.7)), the leading eigenvalue is $\lambda_{\max} = \frac{\beta^2}{4\kappa}$. We now increment the value a by some small step Δa , and compute the corresponding period $p(a + \Delta a)$, using (2.6). The leading eigenvalue for $\bar{\phi}(x; a + \Delta a)$ will be just below the leading eigenvalue for $\bar{\phi}(x; a)$, so we search for zeros of $D(\lambda, \xi)$ with values of λ just below λ_{\max} . Repeating this process iteratively we obtain the leading eigenvalues. For $\alpha = 1$, $\beta = 1$, and $\kappa = 0.001$, a plot of leading eigenvalues as a function of amplitude a is depicted in Figure 5 for two different values of κ .

According to [15], the period $p(t)$ associated with an evolving solution of (2.1) evolves approximately according to the relation

$$\frac{dp}{dt} = \lambda_{\max}(p)p, \quad p(t_0) = p_0, \quad (4.5)$$

where $\lambda_{\max}(p)$ denotes the maximum eigenvalue associated with the specified periodic solution $\bar{\phi}(x; a(p))$.

Remark 4.2. *In the derivation of (4.5) in [15], a small modification to Langer's framework is employed. Precisely, the equation arising from a more faithful adaptation of Langer's original relations is*

$$\frac{dp}{dt} = \frac{1}{2}\lambda_{\max}(p)p, \quad p(t_0) = p_0. \quad (4.6)$$

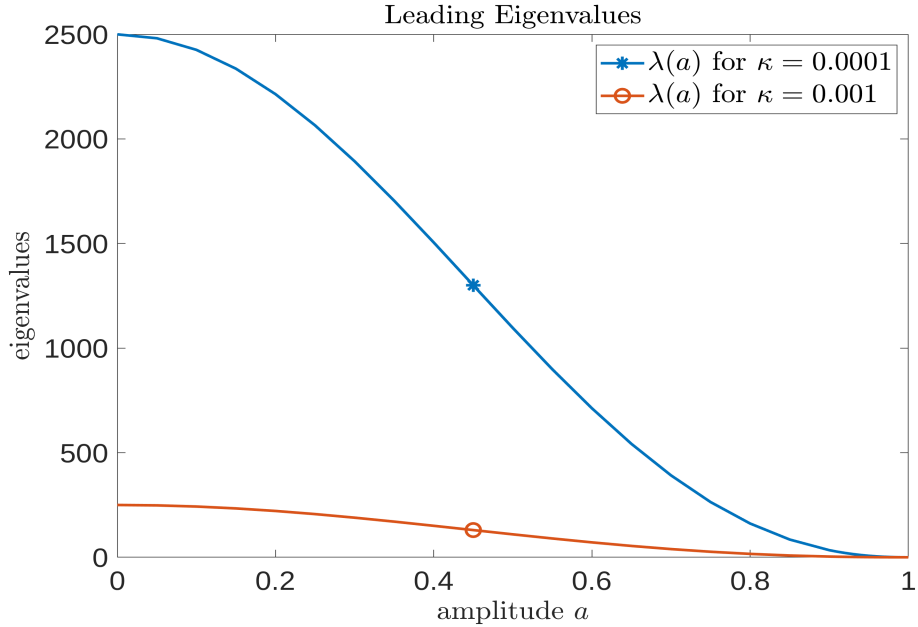


Figure 5: Plot of leading eigenvalues versus amplitude, computed with $\alpha = \beta = 1$, and $\kappa = 0.001$ and $\kappa = 0.0001$.

As a side note to our analysis, we will compare how these two possible methods compare with numerically generated solutions.

If Langer's method and the eigenvalue method are both initialized by the minimum period p_{\min} (from (2.7)), the evolution in time proceeds as in Figure 6b (computed for $\alpha = \beta = 1$, $\kappa = 0.001$). Using $\mathcal{E}(p)$ to map periods to energies, we can evolve energy as a function of time for both Langer's method and the eigenvalue method. This is depicted in Figures 6a and 6b. In order to see that the primary difference between the two approaches is a matter of scaling, we included similar plots using (4.6) in place of (4.5), labeled with the tag, “(1/2 factor)” in Figures 6a and 6b.

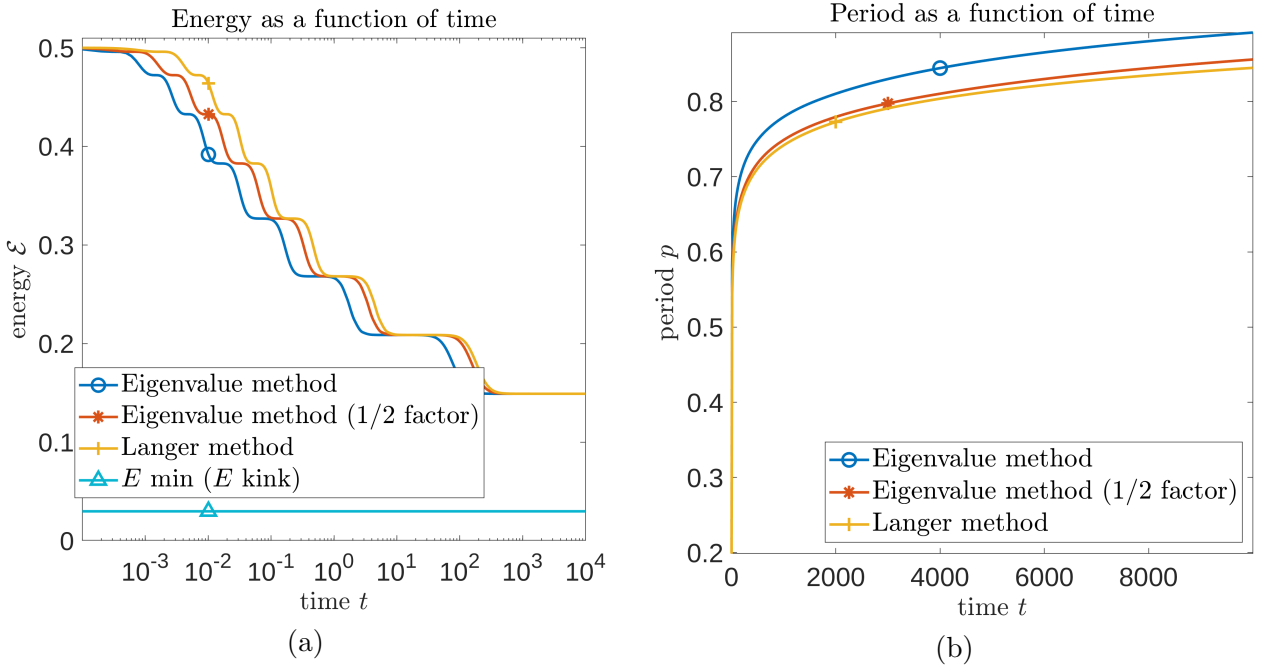


Figure 6: Evolution of energies (a) and periods (b) via Langer's method and the eigenvalue method. For the plots labeled “Eigenvalue method,” equation (4.5) was used. For the plots with the tag “(1/2 factor)”, equation (4.6) (with the extra $\frac{1}{2}$ -factor) was used (cf. Remark 4.2).

4.1 Varying κ

In this section, we observe that it is straightforward to vary κ in the above energy calculations. First, we note that for a fixed interval $[-L, +L]$ the maximum energy specified in (2.8) does not depend on κ . On the other hand, the minimum energy specified in Item (iv) of Proposition 2.4 is proportional to $\sqrt{\kappa}$. For evolution on bounded domains, transition layers are typically removed through the boundary in pairs, so we expect to see energy drops in steps of size $2E_{\min}$. For $\alpha = 1$, $\beta = 1$, and $L = 1$, if $\kappa = 0.001$ then $2E_{\min} = 0.0596$, and likewise if $\kappa = 0.0001$, then $2E_{\min} = 0.0189$, and if $\kappa = 0.00001$, then $2E_{\min} = 0.0060$. Since the energy declines in steps of these sizes, energy plots such as the two depicted in Figure 7 have less pronounced steps for smaller values of κ .

For Langer's approach, dependence on κ is explicit in (4.1), and so changes in κ are readily accommodated. For the eigenvalue approach, we need to identify how the leading eigenvalues vary with κ . To this end, we fix a choice of F with the form (2.2), and we observe that if $\bar{\phi}(x)$ denotes a periodic solution of (2.1) obtained with $\kappa = 1$, then for any $\kappa > 0$, $\bar{\phi}^\kappa(x) := \bar{\phi}(x/\sqrt{\kappa})$ is a periodic solution of (2.1) obtained with the value κ . Upon linearization of (2.1) about $\bar{\phi}^\kappa(x)$, we arrive at the eigenvalue problem

$$(-\kappa\psi'' + F''(\bar{\phi}^\kappa(x))\psi)'' = \lambda\psi.$$

We can express this equation as

$$(-\kappa\psi'' + b(x/\sqrt{\kappa})\psi)'' = \lambda\psi,$$

where $b(x/\sqrt{\kappa}) = F''(\bar{\phi}(x/\sqrt{\kappa}))$, and we can also express this as

$$-\kappa\psi'''' + \frac{1}{\kappa}b''(x/\sqrt{\kappa})\psi + \frac{2}{\sqrt{\kappa}}b'(x/\sqrt{\kappa})\psi' + b(x/\sqrt{\kappa})\psi'' = \lambda\psi.$$

At this point, we make the change of variables

$$y = \frac{x}{\sqrt{\kappa}}, \quad \Psi(y) = \psi(x) \implies \psi^{(k)}(x) = \frac{1}{\kappa^{k/2}}\Psi^{(k)}(y), \quad k = 1, 2, 3, \dots$$

Upon substitution, we see that the equation for $\Psi(y)$ is

$$-(\Psi'' + b(y)\Psi)'' = \kappa\lambda\Psi.$$

We take from this that λ is an eigenvalue for the equation with general κ if and only if $\kappa\lambda$ is an eigenvalue for the equation with $\kappa = 1$. This observation allows us to compute leading eigenvalues for any fixed $\kappa > 0$, and obtain leading eigenvalues associated with all other values of κ by an appropriate scaling argument. To make this precise, suppose that for a specific value κ_0 , we compute the leading eigenvalue λ_0 associated with the periodic solution with amplitude a . Then $\kappa_0\lambda_0$ will be the leading eigenvalue associated with the periodic solution with amplitude a arising as a solution to (2.1) with $\kappa = 1$. Correspondingly, the leading eigenvalue associated with the periodic solution with amplitude a arising as a solution to (2.1) with any general value $\kappa > 0$ will be $(\kappa_0/\kappa)\lambda_0$. In fact, we have already seen an example of this scaling effect in Figure 5.

In Figure 7, we apply these ideas to generate for comparison plots of energy as a function of time for both Langer's method and the eigenvalue method for three values of κ , namely $\kappa = 0.001$, $\kappa = 0.0001$, and $\kappa = 0.00001$. In each case, the energy at $t = 0$ is the same maximum energy $E_{\max} = 0.5$, but the plots are depicted starting with $t = 0.01$, at which point the energies have already declined at varying rates. (These calculations use (4.5) rather than (4.6).)

5 Computational Results

In this section, we consider constant mobility $M \equiv 1$ since the qualitative dynamics do not vary much as long as the mobility is non-degenerate.

5.1 Overview of the numerical methods

Here, we give a brief summary of the numerical methods used throughout this analysis. As much as possible, we have used standard well-established methods, as our goal is not to focus on developing numerical methods, but on understanding dynamical phenomena.

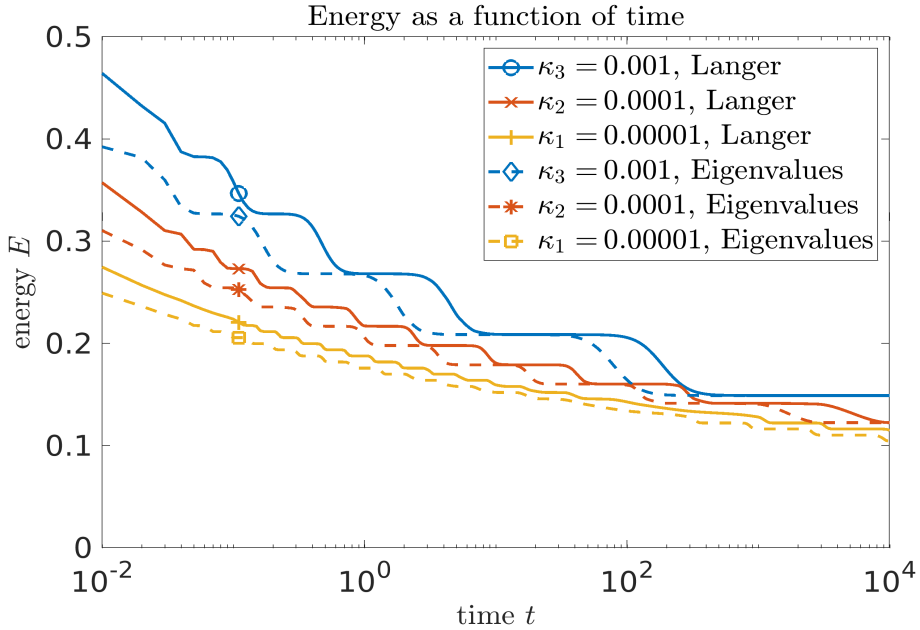


Figure 7: Evolution of energies via Langer’s method and the eigenvalue method for various values κ .

Remark 5.1 (Periodic Domain vs. Full Space). *While the primary focus of the present work is in the full space \mathbb{R} , for the numerical simulations, we work in the periodic domain $[-1, 1]$. Working in a periodic domain yields spectral accuracy for smooth, localized profiles without introducing boundary layers or buffer-zones. By contrast, so-called “full-space discretization” methods (e.g., sinc-type methods on \mathbb{R} , or a nonperiodic truncation to $[-L_*, L_*]$ as $L_* \rightarrow \infty$, or a remapping of \mathbb{R} to a finite interval) come with their own problems, which we now discuss briefly. Sinc methods (see, e.g., [18, 21]) can enjoy spectral accuracy, but to achieve this, one must delicately choose both the grid spacing and the number of nodes carefully to match the unknown strip of analyticity, which poses non-trivial difficulties that would take away from the focus of the present work. Moreover, the differentiation matrix is dense, and can impose severe timestep restrictions. Finally, sinc methods require the solution to decay to zero as $|x| \rightarrow \infty$, and hence to recover, e.g., the kink solution (2.11), one must impose some type of smooth cut-off function anyway. Similar problems arise with remapping \mathbb{R} to a finite interval, which moreover introduces non-constant coefficients and can introduce undesirable “endpoint clustering” (if one discretizes with, e.g., Chebyshev polynomials). Truncation methods must impose artificial boundary conditions at $x = \pm L_*$ leading to loss of accuracy, and can introduce extra tuning parameters (such as the truncation length L_* or the placement of ghost nodes) and often exhibit slower convergence and stability issues due to the nonlinear terms. Hence, for the sake of both simplicity and accuracy, our simulations are carried out in the periodic domain, with the usual adjustments in understanding that come with*

considering dynamics in full space vs. periodic boundary conditions. Note also that we still consider comparison with the full-space “kink” solution (2.11). In the parameter regimes we consider, this solution has interfaces whose deviations from ± 1 decay exponentially fast as $|x| \rightarrow \infty$. When we restrict to $[-1, 1]$ with periodic boundary conditions, truncating to $[-1, 1]$ with periodic boundary conditions incurs an L^∞ error of order $\mathcal{O}(\exp(-2\sqrt{\frac{\beta}{2\kappa}}))$, which is numerically negligible ($\approx 10^{-20}$) for the β, κ values used in our simulations. When the solution evolves, the discontinuity at the periodic boundary quickly vanishes and the solution becomes periodic, but otherwise stays near the kink solution in L^2 norm, although the free energy differs by roughly E_{\min} due to the additional transition layer at the periodic boundary. Thus, although our analysis is focused on full space, periodic computations on $[-1, 1]$ can give a reasonable picture of the dynamics, and using this setting has at least some advantages over “full-space discretizations” as described above.

All simulations were run using MATLAB version 2024a. The spatial discretization was done using standard spectral methods, based on MATLAB’s `fft` and `ifft` (the latter computed using the ‘`symmetric`’ option). Time-stepping was handled by a semi-implicit Euler method. Eyre’s convex splitting method [6, 7] was employed (in particular, algorithm 5, the “Linearly Stabilized Splitting Scheme” proposed in [7]), with the cubic term computed using co-location (i.e., multiplication in physical space). Due to the presence of the cubic term, the highest half of the wave modes were dealiased (i.e., set to zero before being transformed back to physical space). Spatial resolution on the domain $[-1, 1]$ was chosen to be $N = 8192$, giving a spatial stride of $\Delta x = 2\pi/N \approx 7.6699 \times 10^{-4}$. The time-step $\Delta t \approx 9.7656 \times 10^{-5}$ was chosen to respect standard CFL conditions. For simplicity, we chose $\alpha = \beta = K = 1$. Our smallest choice of interfacial energy $\kappa \geq 0.00001$, was found experimentally using the resolution criterion that the energy spectra of dealiased modes of ϕ must be below machine precision ($\approx 2.2204 \times 10^{-16}$) at all time steps after roughly time $t \approx 0.001$ (obviously, since we are starting with normally-distributed random values at each point, the initial data, and consequentially the first few time steps, are not expected to satisfy this criterion).

We often initialize the equation with “random” initial data, which has been evolved until the free energy is just below $0.99E_{\max}$, our tolerance taken somewhat arbitrarily to be 10^{-4} , where $E_{\max} := \frac{\beta^3 L}{4\alpha}$. This is carried out in the following way. First, for the purposes of easy replication of our results, we seed the random number generator (RNG) with seed 0, then we take normally-distributed mean-zero data at each of the N points in space with standard deviation 0.1 (i.e., $\mathcal{N}(0, 0.1)$). The result is then transformed with the discrete Fourier transform, where the upper $N/2$ wave modes are removed (for dealiasing the cubic term). For clarity, the MATLAB code used for this operation is as follows:

```

rng(0, 'twister');
phi_hat = fft(0.1*randn(1,N));
phi_hat((N/4+1):(3N/4+1)) = 0;
phi = ifft(phi_hat, 'symmetric');

```

In our simulations, we used $N = 2^{11} = 2048$ and $L = \alpha = \beta = 1$. The RNG was only seeded by zero on the first trial. On subsequent trials, the seed was determined by whatever the previous state of the system was. After the initialization of ϕ described above, the simulation was then run until free energy satisfied the criterion stated above. For this last stage, we used a variable time-step: if the free energy was not within the desired tolerance of $0.99E_{\max}$, the time step was thrown out and recomputed with half the previous time-step. Once this process was completed, the result was used to initialize our Cahn–Hilliard simulations.

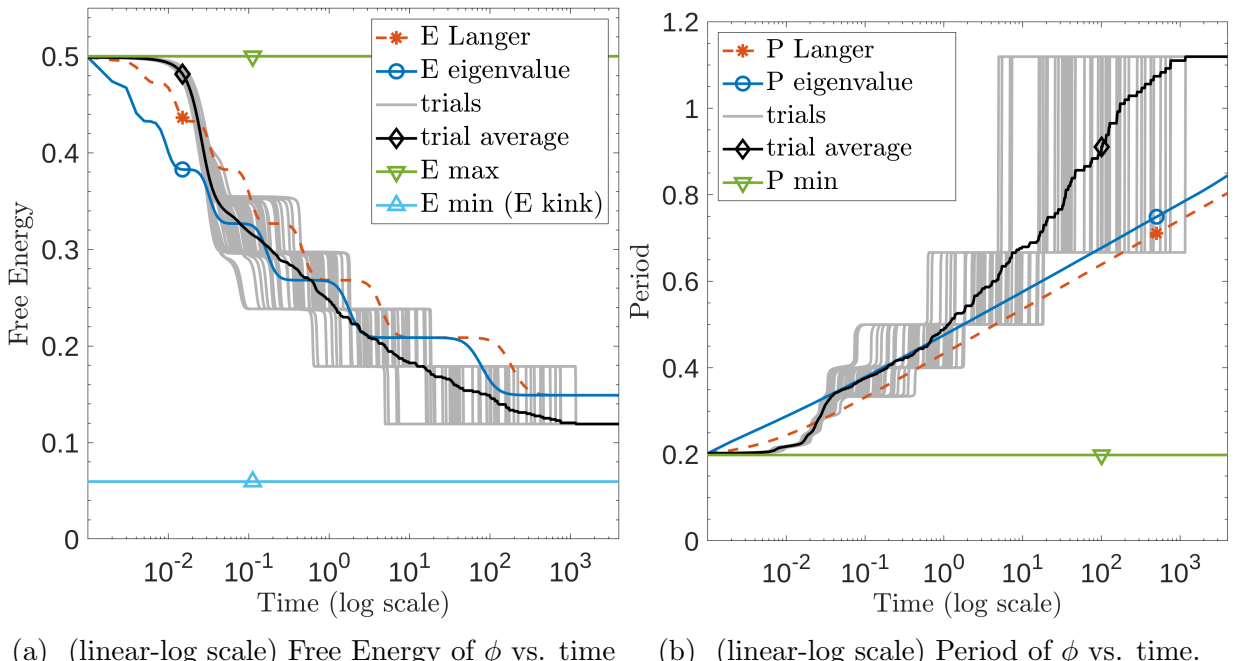
5.2 Simulations for the Cahn–Hilliard Equation

We now carry out our direct computations for the Cahn–Hilliard equation, emphasizing the energy evolution and associated coarsening dynamics. In Figure 8, we depict energies (Figure 8a) and periods (Figure 8b) for 50 trials of the Cahn–Hilliard equation—trials in gray, average in thicker black—along with energies and periods computed with the two analytical methods described in Section 4. For the computationally generated values, initial data for each trial was computed pseudo-randomly as described in Section 5.1, except with the random number generator seeded randomly each time, using `rng(randi(10000))`. The free energy was computed for each trial at each time-step, and the mean of these curves was computed and displayed in Figure 8a. This is the first direct quantitative comparison that we are aware of for the energies obtained from these three approaches, and we interpret the consistency of the results at once as a justification of Langer’s approach in [17] (and subsequently as modified in [15]) and a verification that our computations are faithfully capturing dynamics of the energy. We observe that the horizontal shelves for the three plots occur approximately at integer multiples of the minimum energy, and correspond with the number of transitions in the solution at that point. For the two analytic methods, the underlying periodic solutions are centered with a transition passing through $x = 0$, so by symmetry each shelf will correspond with an odd multiple of the minimum energy (i.e., there will be a transition at $x = 0$ and the same number of transitions to the right and left of this). For the computed energies, periodicity requires an even number of transitions, so the horizontal shelves occur at even multiples of the minimum energy. Notably, this means that the analytic curves will approach E_{\min} asymptotically while the computed curves will approach $2E_{\min}$ asymptotically. In particular, it’s clear that the analytic curves are only transiently above the computed curve.

In Figure 8b, we depict the evolution of the periods associated with the energies in Figure 8a. For the two analytic methods, these periods are computed directly from (4.1) (Langer’s method) and (4.6) (eigenvalue method), while for the computational approach the periods are computed from the energies via the pseudoinverse as specified in Definition 3.2 (though see the caption of Figure 8 for a note on this). The relatively large discrepancy in the latter stages of the evolution is the result of long shelves in $E(p)$, as depicted in Figure 3. As noted in the previous paragraph, the analytic energy will asymptotically pass below the computed energy, and correspondingly the analytic values for coarseness will become larger than the

computed values.

Since the two analytic models were developed by considering (2.1) on \mathbb{R} , it's natural to expect a better correspondence for larger intervals $[-L, L]$. In order to see that this is indeed the case, we include in Figure 9 plots of energies and periods computed for $L = 10$ (and keeping $\kappa = .001$). The horizontal shelves are again separated by steps of size $2E_{\min}$, but these steps are now relatively quite small, and we see close correlation especially between the method of [15] and the computed values. Once again, the coarseness obtained by computation trends slightly below the coarseness obtained from the analytic models for later times in the figure, but we again note that ultimately this will switch so that asymptotically the coarseness obtained from computation will be slightly above the coarseness obtained from the analytic models. Unfortunately, the time expected to see this final switch with parameter values $L = 10$ and $\kappa = .001$ is about 10^{18} , so no such plot was attempted. Rather, we include in Figure 10 a simple plot obtained for $L = 1$ and the larger value $\kappa = .01$ to illustrate the expected time-asymptotic behavior.



(a) (linear-log scale) Free Energy of ϕ vs. time (b) (linear-log scale) Period of ϕ vs. time.

Figure 8: Free energy and periods of 50 trials of the Cahn-Hilliard equation ($\kappa = 0.001$, $\alpha = \beta = 1$, $N = 2^{11} = 2048$, Domain: $[-1, 1]$, $\Delta t = 0.001$, final time $T = 4000$), and the average of these, along with the maximum free energy (2.8), the kink energy (2.12), and the Langer and eigenvalue predictions. In principle, the computational plots in Figure (b) should be generated by applying the pseudoinverse map from Definition 3.2 to the plots in Figure (a), but in practice we found it more efficient to generate a map by interpolating periods as a function of energies. It is clear from our discussion in Section 3 that the two approaches must give nearly identical results.

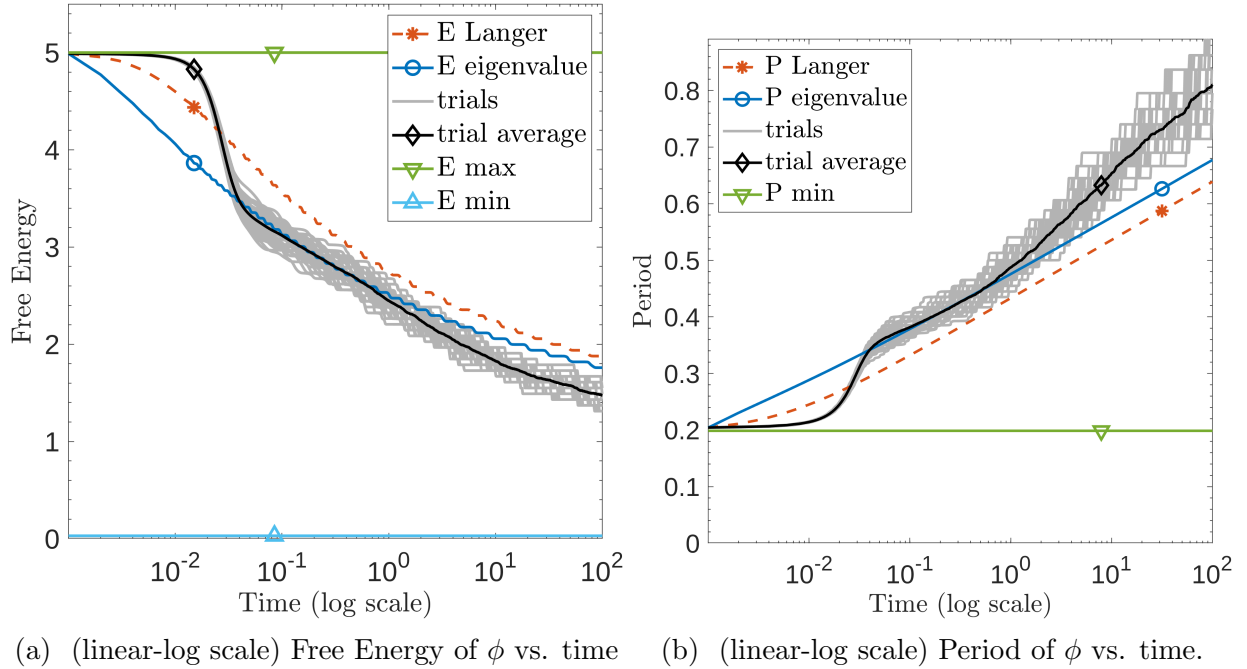
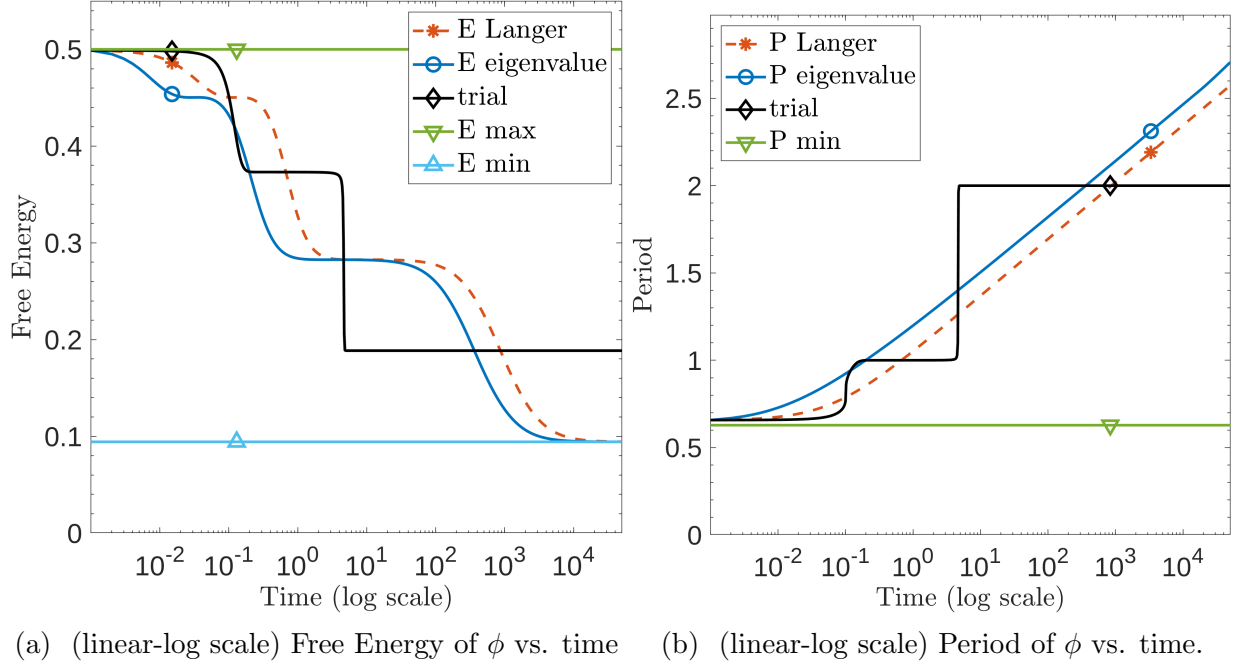


Figure 9: Free energy and periods of 50 trials of the Cahn-Hilliard equation ($\kappa = 0.001$, $\alpha = \beta = 1$, $N = 2^{13} = 8192$, Domain: $[-10, 10]$, $\Delta t = 0.001$, final time $T = 100$), and the average of these, along with the maximum free energy (2.8), the kink energy (2.12), and the Langer and eigenvalue predictions.



(a) (linear-log scale) Free Energy of ϕ vs. time (b) (linear-log scale) Period of ϕ vs. time.

Figure 10: Free energy and periods of 1 trial of the Cahn-Hilliard equation ($\kappa = 0.01$, $\alpha = \beta = 1$, $N = 2^{11} = 2048$, Domain: $[-1, 1]$, $\Delta t = 0.001$, final time $T = 50,000$), along with the maximum free energy (2.8), the kink energy (2.12), and the Langer and eigenvalue predictions. As expected, we see in (a) that the eigenvalue and Langer predictions, which are based on the full-space domain, drop below the trial simulation's lowest energy state, as it is on the periodic domain, and therefore has one additional kink.

6 Conclusion

In this paper, we have introduced a new measure of coarseness for processes modeled by Cahn–Hilliard equations, and used this measure to compare two analytic descriptions of coarsening with computationally generated dynamics. Notably, our measure of coarseness circumvents the need for any *a priori* assumptions about the structure of the solution, such as near-periodicity, allowing us to associate a value of coarseness with any solution to (2.1).

In future work, we plan to use our measure of coarseness to investigate coarsening dynamics in systems obtained when Cahn–Hilliard equations are coupled with a fluids equation to create a model of two-phase flow. In particular, we will start by coupling the Cahn–Hilliard equations considered here with the viscous Burgers equation—creating a natural one-dimensional analog of the Cahn–Hilliard–Navier–Stokes system. Our expectation is that coupling will have a substantial effect on coarsening rates, and our goal will be to meaningfully quantify this effect. We will also study theoretical properties of the coupled Burgers–Cahn–Hilliard equations, such as global well-posedness. Our long-term goal is to extend our study to multi-dimensional Cahn–Hilliard Systems, the Cahn–Hilliard–Navier–Stokes system, and other related equations. Although our 1D investigations point toward promising directions to pursue in such studies, we expect new phenomena to emerge in those cases. In particular, new analytic tools are needed for higher dimensional cases in order to evaluate and analyze coarsening rates.

A Appendix: Proofs of Propositions 2.3 and 2.4

Proof of Proposition 2.3. In order to abbreviate notation, we will write

$$p(a) = 2\sqrt{2\kappa}\tilde{p}(a), \quad \tilde{p}(a) = \int_0^a \frac{dy}{\sqrt{F(y) - F(a)}}.$$

By setting $z = y/a$, we can express $\tilde{p}(a)$ as

$$\tilde{p}(a) = \int_0^1 \frac{a}{\sqrt{F(az) - F(a)}} dz,$$

for which we can justify differentiating through the integral. This gets us to the relation

$$\tilde{p}'(a) = \int_0^1 \frac{(F(az) - \frac{az}{2}F'(az)) - (F(a) - \frac{a}{2}F'(a))}{(F(az) - F(a))^{3/2}} dz. \quad (\text{A.1})$$

In order to establish positivity of $\tilde{p}'(a)$, we will set

$$G(y) := F(y) - \frac{y}{2}F'(y),$$

and show that $G(az) - G(a)$ is positive for all $z \in (0, 1)$. First, $G'(y) = \frac{1}{2}F'(y) - \frac{y}{2}F''(y)$, so in particular $G'(0) = \frac{1}{2}F'(0) = 0$. Next, by assumption, $G''(y) = -\frac{y}{2}F'''(y) < 0$ for all $y \in (0, a)$, so $G'(y)$ is a decreasing function, and we must have $G'(y) < 0$ for all $y \in (0, a)$. It follows that $G(y)$ is a decreasing function, so $G(a) < G(az)$ for all $z \in (0, 1)$, giving the second claim.

For the first claim, it is convenient to return to $y = az$ and rearrange (A.1) as

$$\tilde{p}'(a) = \int_0^a \frac{\frac{1}{2}(F'(a) - F'(y)) + \frac{1}{a}(F(y) - F(a))}{(F(y) - F(a))^{3/2}} dy + \frac{1}{2} \lim_{\tau \rightarrow a^-} \int_0^\tau \frac{F'(y) - \frac{y}{a}F'(y)}{(F(y) - F(a))^{3/2}} dy, \quad (\text{A.2})$$

where the final integral has been expressed as a limit to justify integrating by parts. Integrating by parts, we find

$$\begin{aligned} \lim_{\tau \rightarrow a^-} \int_0^\tau \frac{F'(y) - \frac{y}{a}F'(y)}{(F(y) - F(a))^{3/2}} dy &= - \int_0^a \frac{\frac{2}{a}(F(y) - F(a))}{(F(y) - F(a))^{3/2}} dy + \lim_{\tau \rightarrow a^-} \frac{-2(1 - \frac{y}{a})}{\sqrt{F(y) - F(a)}} \Big|_0^\tau \\ &= - \int_0^a \frac{\frac{2}{a}(F(y) - F(a))}{(F(y) - F(a))^{3/2}} dy + \frac{2}{\sqrt{F(0) - F(a)}}. \end{aligned}$$

Recalling the factor of $1/2$, we see that the first summand on the right-hand side of this last expression cancels with the second part of the first integral on the right-hand side of (A.2), leaving

$$\tilde{p}'(a) = \frac{1}{\sqrt{F(0) - F(a)}} + \int_0^a \frac{\frac{1}{2}(F'(a) - F'(y))}{(F(y) - F(a))^{3/2}} dy.$$

Recalling the specification $p(a) = 2\sqrt{2\kappa}\tilde{p}(a)$, we see that the proof is complete. \square

Proof of Proposition 2.4. Items (i) and (ii) are clear from evaluation of the indicated formulas at the specific family of bulk free energy densities (2.2). For Item (iii), we first observe that for F as specified in (2.2), we can write

$$F(y) - F(a) = \left(\frac{\alpha}{4}y^2 + \frac{F(a) - F(0)}{a^2} \right) (y^2 - a^2).$$

In this case, (2.5) becomes

$$\int_0^{\bar{\phi}(x;a)} \frac{dy}{\sqrt{\frac{2}{\kappa}(\frac{\alpha}{4}y^2 + \frac{F(a) - F(0)}{a^2})(y^2 - a^2)}} = x.$$

In order to express this as a Jacobi elliptic function, we first multiply both sides by the factor $(1/a)\sqrt{-2(F(a) - F(0))/\kappa}$ to obtain

$$\int_0^{\bar{\phi}(x;a)} \frac{\frac{1}{a}\sqrt{\frac{-2(F(a) - F(0))}{\kappa}}}{\sqrt{\frac{2}{\kappa}(\frac{\alpha}{4}y^2 + \frac{F(a) - F(0)}{a^2})(y^2 - a^2)}} dy = \frac{x}{a}\sqrt{\frac{-2(F(a) - F(0))}{\kappa}},$$

which we can rearrange to

$$\int_0^{\bar{\phi}(x;a)} \frac{dy}{\sqrt{(a^2 - y^2)(1 + \frac{\alpha a^2}{4(F(a) - F(0))} y^2)}} = \frac{x}{a} \sqrt{\frac{-2(F(a) - F(0))}{\kappa}}.$$

If we now set $y = a \sin \theta$ and specify k as in (2.10), we obtain the relation

$$\int_0^{\bar{\theta}(x;a)} \frac{d\theta}{\sqrt{1 - k^2 \sin^2 \theta}} = \frac{x}{a} \sqrt{\frac{-2(F(a) - F(0))}{\kappa}},$$

where $\sin \bar{\theta} = \bar{\phi}/a$. By definition of the Jacobi elliptic function sn (see Remark 2.5),

$$\text{sn} \left(\sqrt{\frac{-2(F(a) - F(0))}{\kappa}} \frac{x}{a}, k \right) = \sin \bar{\theta}(x; a) = \frac{\bar{\phi}(x; a)}{a},$$

from which Item (iii) follows immediately.

Turning to Item (iv), it is straightforward to verify directly that (2.11) is indeed a stationary solution to (2.1) with F as in (2.2). For the energy claim, we need to evaluate E in (2.3) at $K(x)$. For this, we first observe that $K(x)$ satisfies the equation

$$K' = \sqrt{\frac{2}{\kappa} F(K(x))},$$

so that

$$E(K(x)) = \int_{-L}^{+L} F(K(x)) + \frac{\kappa}{2} \cdot \frac{2}{\kappa} F(K(x)) dx = 2 \int_{-L}^{+L} F(K(x)) dx.$$

We make the change of variables $y = K(x)$, so that

$$dy = K'(x) dx = \sqrt{\frac{2}{\kappa} F(K(x))} dx,$$

giving

$$\begin{aligned} E(K(x)) &= \sqrt{2\kappa} \int_{K(-L)}^{K(+L)} \sqrt{F(y)} dy = \sqrt{\frac{\kappa\alpha}{2}} \int_{K(-L)}^{K(+L)} \frac{\beta}{\alpha} - y^2 dy \\ &= \sqrt{2\kappa\alpha} K(L) \left(\frac{\beta}{\alpha} - \frac{K(L)^2}{3} \right), \end{aligned}$$

where in obtaining the final equality, we integrated directly and observed the relation $K(-L) = -K(L)$. Finally, the statement about E_{\min}^∞ is clear from the limit

$$\lim_{L \rightarrow \infty} K(L) = \sqrt{\frac{\beta}{\alpha}}.$$

□

Acknowledgments

The authors would like to thank editors and the reviewers for their insightful and constructive comments, which have helped us to improve significantly the quality of the paper. A.L. was supported in part by NSF grants DMS-2206762, DMS-2510494, and CMMI-1953346, and USGS Grant No. G23AC00156-01. Q.L. was partially supported by the Simons Foundation (SFI-MPS-TSM-00013384).

References

- [1] J. Bricmont, A. Kupiainen, and J. Taskinen. Stability of Cahn–Hilliard fronts. *Comm. Pure Appl. Math.*, LII:839–871, 1999.
- [2] J. W. Cahn. On spinodal decomposition. *Acta. Metall.*, 9:795–801, 1961.
- [3] J. W. Cahn and J. E. Hilliard. Free energy of a nonuniform system I: Interfacial free energy. *J. Chem. Phys.*, 28:258–267, 1958.
- [4] E. Carlen, M. Carvalho, and E. Orlandi. A simple proof of stability of fronts for the Cahn–Hilliard equation. *Commun. Math. Phys.*, 224:323–340, 2001.
- [5] C. L. Emmott and A. J. Bray. Coarsening dynamics of a one-dimensional driven Cahn–Hilliard system. *Phys. Rev. E*, 54:4568–4575, 1996.
- [6] D. J. Eyre. Unconditionally gradient stable time marching the Cahn–Hilliard equation. *Comm. Math. Models Microstruct. Evol.*, 53:1686–1712, 1998.
- [7] D. J. Eyre. An unconditionally stable one-step scheme for gradient systems, 1998. Unpublished article. <http://www.math.utah.edu/~eyre/research/methods/stable.ps>.
- [8] H. Garcke, B. Niethammer, M. Rumpf, and U. Weikard. Transient coarsening behavior in the Cahn–Hilliard model. *Acta Mater.*, 51:2823–2830, 2003.
- [9] R. A. Gardner. On the structure of the spectra of periodic travelling waves. *J. Math. Pures Appl.*, 72:415–439, 1993.
- [10] R. A. Gardner. Spectral analysis of long wavelength periodic waves and applications. *J. Reine Angew. Math.*, 491:149–181, 1997.
- [11] C. P. Grant. *The dynamics of pattern selection for the Cahn–Hilliard equation*. PhD thesis, The University of Utah, 1991.
- [12] C. P. Grant. Spinodal decomposition for the Cahn–Hilliard equation. *Comm. Partial Differential Equations*, 18:453–490, 1993.

- [13] P. Howard. Asymptotic behavior near transition fronts for equations of generalized Cahn–Hilliard form. *Comm. Math. Phys.*, 269:765–808, 2007.
- [14] P. Howard. Spectral analysis of stationary solutions of the Cahn–Hilliard equation. *Adv. Diff. Eqns.*, 14:87–120, 2009.
- [15] P. Howard. Spectral analysis for periodic solutions of the Cahn–Hilliard equation on \mathbb{R} . *Nonlinear Differ. Equ. Appl.*, 18:1–26, 2011.
- [16] R. V. Kohn and F. Otto. Upper bounds on coarsening rates. *Comm. Math. Phys.*, 229:375–395, 2002.
- [17] J. S. Langer. Theory of spinodal decomposition in alloys. *Ann. Phys.*, 65:53–86, 1971.
- [18] J. Lund and K. L. Bowers. *Sinc Methods for Quadrature and Differential Equations*. SIAM, 1992.
- [19] F. W. J. Olver, A. B. O. Daalhuis, D. W. Lozier, B. I. Schneider, R. F. Boisvert, C. W. Clark, B. R. Miller, B. V. Saunders, H. S. Cohl, and M. A. McClain, editors. *NIST Digital Library of Mathematical Functions*. National Institute of Standards and Technology, release 1.2.0 edition, 2024. <https://dlmf.nist.gov/>, Release date: 2024-03-15.
- [20] F. Otto and M. G. Westdickenberg. Relaxation to equilibrium in the one-dimensional Cahn–Hilliard equation. *SIAM J. Math. Anal.*, 46(1):720–756, 2014.
- [21] F. Stenger. *Handbook of Sinc Numerical Methods*. CRC Press, 2016.
- [22] S. J. Watson, F. Otto, B. Y. Rubinstein, and S. H. Davis. Coarsening dynamics of the convective Cahn–Hilliard equation. *Phys. D*, 178(3-4):127–148, 2003.